Journal of Ethnopharmacology 268 (2021) 113668

Contents lists available at ScienceDirect

Journal of Ethnopharmacology

journal homepage: www.elsevier.com/locate/jethpharm

Anti-inflammatory, pro-proliferative and antimicrobial potential of the compounds isolated from *Daemonorops draco* (Willd.) Blume

L. Apaza Ticona [a,b,*], Á. Rumbero Sánchez [a], J. Sánchez Sánchez-Corral [a], P. Iglesias Moreno [b], M. Ortega Domenech [c]

[a] Department of Organic Chemistry, Faculty of Sciences, Universidad Autónoma de Madrid, Cantoblanco, 28049, Madrid, Spain
[b] Department of Pharmacology, Pharmacognosy and Botany, Faculty of Pharmacy, Universidad Complutense de Madrid, Plza. Ramón y Cajal S/n, 28040, Madrid, Spain
[c] Dr. Goya Análisis, SL, Alcalá de Henares, 28805, Madrid, Spain

ARTICLE INFO

Keywords:
Daemonorops
Dragon's blood
Wound healing
Anti-inflammatory
Pro-proliferative
Antimicrobial

ABSTRACT

Ethno-pharmacological relevance: Daemonorops draco (*D. draco*) commonly known as "Dragon's blood" is one of the most used plants by Momok, Anak Dalam and Talang Mamak tribes from Indonesia as a remedy for wound healing.

Aim of the study: This study aimed to identify the extract, fractions and compounds responsible for the anti-inflammatory and pro-proliferative activities of the *D. draco* resin. Additionally, the antimicrobial activity against two bacteria and one yeast species was analysed.

Materials and methods: Bio-guided isolation of compounds with anti-inflammatory, pro-proliferative and antimicrobial activities from the *D. draco* resin was carried out by measuring: the inhibition of NF-κB and activation of Nrf2 in THP-1, HaCaT, NIH-3T3 cells; cell proliferation in NIH-3T3 and HaCaT cells; and the antimicrobial effect on *E. coli*, *S. aureus* and *C. albicans*.

Results: Guided isolation by bioassay gave rise to the isolation and characterisation by nuclear magnetic resonance and mass spectrometry of three compounds: **1** (Bexarotene), **2** (Taspine) and **3** (2-hydroxy-1-naphthaldehyde isonicotinoyl hydrazone). All compounds showed NF-κB inhibitory activity with IC_{50} values of 0.10–0.13, 0.22–0.24 and 3.75–4.78 μM, respectively, while the positive control, Celastrol, had an IC_{50} of 7.96 μM. Likewise, all compounds showed an activating effect of Nrf2 with EC_{50} values of 5.34–5.43, 163.20–169.20 and 300.82–315.56 *n*M, respectively, while the positive control, CDDO-Me, had an EC_{50} of 0.11 *n*M. In addition, concerning the pro-proliferative activity, compound **1** (IC_{50} = 8.62–8.71 *n*M) showed a capacity of 100%, compound **2** (IC_{50} = 166–171 *n*M) showed a capacity of 75%, and compound **3** (IC_{50} = 469–486 *n*M) showed a capacity of 65%, while FSB 10% (positive control) had a pro-proliferative activity of 100% in the NIH3T3 cell lines (fibroblasts) and HaCaT (keratinocytes).

Finally, all the compounds showed antimicrobial activity with MIC values of 0.12–0.16, 0.31–0.39 and 3.96–3.99 μM, respectively, in *S. aureus*, *E. coli* and *C. albicans* strains, while the positive control, Ofloxacin, had a MIC of 27.65 μM.

Conclusion: This study managed to isolate, for the first time, three compounds (Bexarotene, Taspine and 2-hydroxy-1-naphthaldehyde isonicotinoyl hydrazone) from the resin of *D. draco*, with anti-inflammatory, and pro-proliferative as well as antimicrobial activities.

1. Introduction

Skin is one of the most important organs for the human being since it constitutes the first defence barrier. For this reason, it is continuously exposed to all kinds of external agents that trigger a series of inflammatory reactions (Proksch, 2018; Kabashima et al., 2019). When an injury (wound, abrasion, burn, cut) occurs on the skin, a healing process starts, aiming to repair and regenerate the damaged tissues (Gonzalez et al., 2016; Zhao et al., 2016). This process can be divided in four stages: coagulation, inflammation, proliferation and maturation (Ashrafi et al., 2016; Sami et al., 2019).

* Corresponding author. Luis Apaza Ticona. Department of Organic Chemistry, Faculty of Sciences, Universidad Autónoma de Madrid, Cantoblanco, 28049, Madrid, Spain.
E-mail addresses: luis.apaza@uam.es, lnapaza@ucm.es (L. Apaza Ticona).

https://doi.org/10.1016/j.jep.2020.113668
Received 4 October 2020; Received in revised form 30 November 2020; Accepted 2 December 2020
Available online 8 December 2020

Abbreviations

AcOEt	Ethyl Acetate
ARE	Antioxidant Responsive Element
ATCC	American Type Culture Collection
BOD	Bio-Oxygen Demand
CC_{50}	Cytotoxic Concentration 50%
CDDO-Me	2-Cyano-3,12-dioxo-oleana-1,9-(11)-dien-28-oic acid methyl ester
CFU	Colony-Forming Unit
$CI_{95\%}$	Confidence Interval 95%
DCM	Dichloromethane
DH2O	Distilled Water
DMEM	Dulbecco's Modified Eagle Medium
DMSO	Dimethyl Sulfoxide
DTT	Dithiothreitol
EGF	Epidermal Growth Factor
ELISA	Enzyme-Linked Immunosorbent Assay
EtOH	Ethanol
FBS	Fetal Bovine Serum
HEX	*n*-Hexane
HO-1	Heme Oxygenase 1
IC_{50}	Inhibitory Concentration 50%
LDH	Lactate Dehydrogenase
MeOH	Methanol
MHB	Mueller-Hinton broth
MIC	Minimum Inhibitory Concentration
NBM	Nutrient Broth Medium
NF-κB	Nuclear Factor Kappa-Light-Chain-Enhancer of Activated B Cells
Nrf2	Nuclear Factor Erythroid 2-related Factor 2
PBS	Phosphate-Buffered Saline
QTOF	Quadrupole Time-of-Flight
RLUs	Relative Luminescence Units
ROS	Reactive Oxygen Species
TLC	Thin Layer Chromatography
TMS	Tetramethylsilane
TNF-α	Tumour Necrosis Factor-α
TGF-β	Transforming Growth Factor-β
ZI	Zone of Inhibition

Regarding the inflammation stage, there are reports on the role of pro-inflammatory cytokines released by macrophages in the positive regulation of inflammatory reactions and in the process of the pathological pain (Cavaillon, 2018). In this sense, the pro-proliferative activity is accelerated through adequate temporal downward regulation of pro-inflammatory cytokine levels (Opal and DePalo, 2000). Within cytokines, the NF-κB (Nuclear Factor Kappa-Light-Chain-Enhancer of Activated B Cells) cytokine has a crucial role in the pathogenesis of several inflammatory diseases (Lawrence, 2009).

Additionally, several works suggest the importance of Nrf2 (Nuclear Factor Erythroid 2-related Factor 2) during processes of cell proliferation and differentiation, as well as tissue repairing, regulating protein expression (Ambrozova et al., 2017; Hiebert and Werner, 2019). Keratinocytes of the hyperproliferative epithelium of skin wounds were shown to strongly express Nrf2, but expression of this gene was also described in cells of the granulation tissue (Ambrozova et al., 2017). Nrf2 has also been shown to be activated after tissue damage and synergised with other transcription factors such as NF-κB, enabling the pro-proliferative process (Eichenfield et al., 2016).

Finally, infection is one of the significant causes of delayed wound healing (Gottrup et al., 2013); therefore, infection control should be carefully considered for curing wounds. To control infection, wounds should be treated with aseptic techniques and appropriate antimicrobial agents (Vermeulen et al., 2010). During the infection, pro-inflammatory cytokines (e.g. TNF-α, NF-κB) are important regulators of host responses to microbial challenges (Ziltener et al., 2016). These cytokines amplify and coordinate pro-inflammatory signals that lead to the expression of effector molecules, thus inducing the modulation of the diverse aspects of the innate immunity against infection (Hop et al., 2017).

In this context, the pro-proliferative process can be enabled by natural products with medicinal properties (Fazil and Nikhat, 2020). Different studies have focused on the pro-proliferative properties of natural products with anti-inflammatory, antimicrobial and pro-collagen synthesis properties (Agyare et al., 2019). These medicinal properties can be attributed to the bioactive phytochemical constituents of alkaloids, essential oils, flavonoids, tannins, terpenoids, saponins and phenolic compounds (Georgescu et al., 2016).

Among medicinal plants with pro-proliferative, anti-inflammatory and antimicrobial activities, the plant species called "Dragon's blood" has been studied for its traditional use in different cultures (Egypt, China, India, South America) (Gupta et al., 2007). Among the several species identified as "Dragon's blood" (species of the Croton, Dracaena, Pterocarpus and Daemonorops genera), we will analyse in this work the *Daemonorops draco* species.

Daemonorops draco (Willd) Blume, belonging to the Arecaceae family, is a native species from Indonesia, which has been traditionally used by the Momok, Anak Dalam and Talang Mamak tribes as a remedy for treating wounds because of its anti-haemorrhagic, anti-inflammatory and healing properties (Sulasmi, 2012a, 2012b). The *D. draco* species has been reported to contain triterpenes, flavans, chalcones (Nasini and Piozzi, 1981), diterpene acids (Piozzi et al., 1974) and biflavonoids (Merlini and Nasini, 1976). 57 compounds have been isolated and characterised from the resin of *D. draco*, with 14 out of the 57 compounds showing pharmacological activities. The chloroform, ethyl acetate and methanol extracts have been reported as having antimicrobial (Wahyuni et al., 2018), antioxidant (Purwanti et al., 2019) and anti-inflammatory (Kuo et al., 2017) activities.

This article aims to provide a scientific basis for the traditional use of *Daemonorops draco* as a remedy for wound treatment. In this sense, a bio-guided phytochemical study was carried out to identify those *D. draco* compounds with anti-inflammatory potential (inhibition of NF-κB production and Nrf2 activation) and pro-proliferative activity in NIH-3T3 and HaCaT cells; and with antimicrobial activity in three microbial strains (*Candida albicans*, *Escherichia coli* and *Staphylococcus aureus*).

2. Material and methods

2.1. Plant material

Daemonorops draco was collected from the Baxian Mountain National Nature Reserve, located at the southern slope of the Yanshan mountain chain, northeast of Jixian County, Tianjin, China (40°11′56.4″N and 117°33′60.0″E), in December 2018, at an altitude of 1046.8 m. Botanical identification was confirmed by the Tianjin Natural History Museum, and a voucher specimen was deposited (TJC 0729). The fruits were left to dry for 3 day at a temperature of 25 ± 5 °C, to avoid the compounds from suffering some type of decomposition and/or chemical modification. Subsequently, the crushing and pulverisation was carried out using a knife and hammer mill (Greiffenberger Antriebstechnik GmbH Marktredwitz model), to promote the powdery detachment of the fruit resin. Finally, the resin was sieved to obtain a homogeneous powder with a particle size of 2 mm.

2.2. General experimental procedures

First grade organic solvents were used for isolating the compounds and they were purchased from Sigma-Aldrich. Column chromatography was performed with silica gel (20–45 μm and 40–63 μm, Merck). TLC was performed using Merck Silica gel 60-F_{254} plates. Chromatograms thus obtained were visualised by UV absorbance (254 nm) and through heating a plate stained with a 5% phosphomolybdic acid solution in EtOH 95% (Ethanol 95%) followed by heat application.

NMR experiments were performed on the Bruker Advance DRX 300 and 500 spectrometers operating at 300 MHz, 500 MHz (^{1}H) or 76 MHz, and 126 MHz (^{13}C) with TMS (Tetramethylsilane) as the internal standard. The deuterated solvents were $CDCl_3$-d_1 and MeOD-d_4. Spectra were calibrated by assignment of the residual solvent peak to δ_H 7.26, δ_H 3.31 and δ_C 77.16, δ_C 49.00, for $CDCl_3$ and MeOD, respectively. The complete assignment of protons and carbons was done by analysing the correlated ^{1}H–^{1}H COSY, ^{1}H–^{13}C HSQC and ^{1}H–^{13}C HMBC spectra.

Mass spectra were performed on a mass spectrometer with a QTOF (Quadrupole Time-of-Flight) hybrid model QSTAR *pulsar i analyser* from the commercial company AB Sciex. The samples were analysed using the electrospray ionisation technique in positive and negative ion detection mode. They were introduced into the mass spectrometer by direct infusion at a flow of 10 μL/min, using a syringe pump.

2.3. Extraction and isolation

350 g of the dry powder of the fruits of *D. draco* were extracted by repeated maceration (3 times/24 h/25 °C) with 500 mL of different solvents, increasing the polarity: HEX (*n*-Hexane), DCM (Dichloromethane), MeOH (Methanol) and DH2O (Distilled Water). Subsequently, the extracts were filtered, and the respective solvents were removed by vacuum rotary evaporation at room temperature (25 °C). As a result, four extracts of 8 g, 25 g, 19 g and 6 g, respectively, were obtained.

Dichloromethane extract (20 g) was selected as the most active one and was fractionated using a chromatographic column (4 × 40 cm) with Si-60 Silica gel (40–63 μm, Merck) as a stationary phase and a DCM/MeOH gradient (9.5:0.5 → 0:1) as eluent. A total of eleven fractions (F1–F11) were obtained: F1 (0.169 g), F2 (0.038 g), F3 (0.054 g), F4 (0.084 g), F5 (0.112 g), F6 (0.074 g), F7 (0.075 g), F8 (0.039 g), F9 (0.117 g), F10 (0.233 g) and F11 (0.123 g).

Subsequently, based on the biological activity data, a second separation of F2 was carried out by using a chromatographic column (4 × 40 cm) with Si-60 Silica gel (40–63 μm, Merck) as a stationary phase and a HEX/AcOEt (Ethyl Acetate) gradient (19.5:0.5 → 0:1). A total of eight fractions (I-VIII) were obtained: F2.I (2.3 mg), F2.II (3.1 mg), F2.III (4 mg), F2.IV (1.1 mg), F2.V (3.5 mg), F2.VI (4.3 mg), F2.VII (2.5 mg), and the F2.VIII (6.7 mg) which was the compound RDDDCM-F2. VIII (**1**).

On the other hand, a liquid-liquid extraction was carried out to obtain an extract rich in alkaloids, using the methodology of Tsacheva et al. (2004). 3.80 g of dry powder were left stirring for 30 min with 100 mL of DCM and 50 mL of 6% ammonia. It was then extracted repeatedly with DCM (3 × 100 mL). The organic fractions were combined and concentrated by rotary evaporation to remove the solvent.

The alkaloid-rich dichloromethane extract (1.8 g) showed a pharmacological activity similar to the dichloromethane extract, so it was subjected to column chromatography (3 × 25 cm) on silica gel (20–40 μm) at medium pressure in HEX (125 mL), dioxane and MeOH (250 mL) in a gradient of increasing polarity. The fractions obtained were grouped according to the results of the chromatographic analysis by TLC (Thin Layer Chromatography), obtaining three fractions (F1′-F3'). Further purification of the active fractions (F1' and F2') on silica gel microcolumns yielded the compounds RDDDCM-ALK_F1' (**2**) and RDDDCM-ALK_F2' (**3**).

2.4. Cell culture reagents and drugs

Three cell lines were used in this study: NIH-3T3 (Mouse embryo fibroblast, CRL-1658), HaCaT (Human skin keratinocyte, PCS-200-011) and THP-1 (Human peripheral blood monocyte, TIB-202) cells were used as a negative control to evaluate the cytotoxicity of the samples. All cell lines were obtained from the ATCC (American Type Culture Collection). Cells were cultured in specific media according to ATCC recommendations. The incubation condition for all cells was at an atmosphere of 95% air and 5% CO_2 at 37 °C.

DMEM (Dulbecco's Modified Eagle Medium, Sigma-Aldrich, St. Louis, MO, USA), FBS (Fetal Bovine Serum, Summit Biotechnology; Ft. Collins, CO) and PBS (Phosphate-Buffered Saline, SAFC Biosciences, Inc. Andover-Hampshire, UK) were used as culture mediums. L-glutamine was obtained from Applichem. Penicillin and streptomycin were purchased from Fisher Scientific (Pittsburgh, PA). For cytotoxicity and activity assays the compounds were dissolved in DMSO (Dimethyl Sulfoxide, Merck) at a concentration of 10 mM, while extracts and fractions were dissolved at 20 mg/mL in DMSO.

2.5. Cytotoxicity assay

The samples were determined in a panel of two cell lines (NIH-3T3 and HaCaT) and a control cell line (THP-1) by means of the LDH (Lactate Dehydrogenase) assay at different concentrations (100, 50, 25, 12.5, 6.25, 3.125, 1563, 0.781, 0.391 and 0.95) in μg/mL (extracts and fractions) or μM (compounds). The cells were seeded in 96-well plates at a density of 3 × 10^3 cells/well and incubated overnight at 37 °C in a humidified atmosphere of 5% CO_2. Subsequently, the cells were treated with the extracts or compounds at different concentrations and using DMSO as a control for 48 h. Actinomycin D (≥95% Sigma-Aldrich, CAS Number 50-76-0) was used as a positive control at a concentration of 7.97 *n*M, showing cell death. After 48 h of treatment with the extracts or compounds, 100 μL of culture supernatants were collected and incubated in the reaction mixture of the LDH kit (Innoprot Company). After 30 min, the reaction was stopped by the addition of 1 N HCl, and the absorbance at a wavelength of 490 nm was measured using a spectrophotometric ELISA (Enzyme-Linked Immunosorbent Assay plate reader, SpectraMax® i3, Molecular Devices).

2.6. In vitro anti-inflammatory activity

2.6.1. NF-κB inhibition assay

Cells (3 × 10^3 cells/well) were stably transfected with the KBF-Luc plasmid, which contains three copies of NF-κB binding site (from a major histocompatibility complex promoter), fused to a minimal simian virus 40 promoter driving the luciferase gene. Cells were seeded the day before the assay on 96-well plate. The cells were then treated with samples (extracts, fractions and compounds) at the same concentrations used in the viability assays for 15 min and then they were stimulated with 30 *n*g/mL TNF-α. Celastrol (≥98% Sigma-Aldrich, CAS Number 34157-83-0) was used as a positive control at a concentration of 7.41 μM. After 48 h, the cells were washed twice with PBS and lysed for 15 min in a 50 μL buffer containing 25 mM Tris-phosphate (pH 7.8), 8 mM $MgCl_2$, 1 mM DTT (Dithiothreitol), 1% Triton X-100 and 7% glycerol, at room temperature, using a horizontal shaker. The luciferase activity was measured using a GloMax 96 microplate luminometer (Promega) following the instructions of the luciferase assay kit (Promega, Madison, WI, USA). The RLU (Relative Luminescence Units) was calculated and the results were expressed as percentage of inhibition of NF-κB activity induced by TNF-α (100% activation). The experiments for each concentration of the assay elements were performed in triplicate wells.

2.6.2. Nrf2 activity assay

All cells contained the Nqo1 ARE-Luc reporter plasmid. ARE (Antioxidant Responsive Element) was activated by all members of the CNC

family of factors (Nrf 1, Nrf2, Nrf 3 and p45 NF-E2). The cells were cultivated in 96-well plates at the concentration of 3×10^3 cells/well in a CO_2 incubator at 37 °C. For induction of Nrf2 activation, the cells were treated for 48 h with samples (extracts, fractions and compounds) at the same concentrations used in the viability assays. As a positive control, the cells were treated with CDDO-Me (≥98% Sigma-Aldrich, CAS Number 218600-53-4), used at a concentration of 0.11 *n*M. Then the cells were washed twice in PBS and lysed in 25 mM Tris-phosphate pH 7.8, 8 mM $MgCl_2$, 1 mM DTT, 1% Triton X-100 and 7% glycerol during 15 min at room temperature, using a horizontal shaker. The luciferase activity was measured using a GloMax 96 microplate luminometer (Promega), following the instructions of the luciferase assay kit (Promega, Madison, WI, USA). The results obtained from the lysis buffer were subtracted from each experimental value, and the specific transactivation expressed as fold induction over basal levels (untreated cells). The experiments for each concentration of the assay items were done in triplicate wells.

2.7. Evaluation parameters of the pro-proliferative activity

2.7.1. Real-time pro-proliferative activity assay

NIH-3T3 and HaCaT cells (3×10^3 cells/well) were seeded in a 96-well Essen ImageLock plate (Essen BioScience) and grown to confluence in a CO_2 humidified incubator in the absence of FBS. As a positive control, the cells were treated with 10% FSB (Summit Biotechnology; Ft. Collins, CO). After 24 h, the scratch was made using the 96-pin WoundMaker (Essen BioScience). Wound images were taken every 3 h for 48 h, and the data was analysed with the Relative Wound Density integrated metric. This is part of the IncuCyte HD live content cell imaging system (Essen BioScience).

2.8. In-vitro antimicrobial activity

2.8.1. Microorganisms

In the present study, strains of three microorganisms were used: Gram-positive *Staphylococcus aureus* (ATCC 25904); Gram-negative *Escherichia coli* (ATCC 25922D-5) and *Candida albicans* yeast (ATCC 10231). These three microorganisms were chosen because they are predominant opportunistic pathogens in skin infections (Petkovsek et al., 2009; Kashem and Kaplan, 2016; Hülpüsch et al., 2020).

2.8.2. Agar well diffusion method

For the cultivation of the bacterial strains, NBM (Nutrient Broth Medium) was prepared using 8% nutrient broth in double DH2O and agar-agar. It was subjected to autoclaving at 15 Ibs psi for 30 min/s. Agar plates were prepared by pouring 15 mL of NBM into petri dishes under aseptic condition and kept at room temperature (25 °C) for stabilisation. Bacterial cell cultures were maintained in peptone saline solution by regular sub-culturing and were incubated at 37 °C for 24 h (Apaza et al., 2020).

Agar plates were inoculated by streaking 3 times the swab of bacterial strains over the entire sterile agar surface, and rotating the agar plate at 60° for uniform distribution of the inoculum. The plates were dried at room temperature under aseptic condition followed by boring of 9 mm diameter wells. Serial dilutions (100, 50, 25, 12.5, 6.25, 3.12, 1.56, 0.78, 0.39 and 0.19 μg/mL) of the samples (extracts, fractions and compounds) and standard drug Ofloxacin (27.67 μM) were prepared using DMSO as solvent. The samples (100 μL) were added in wells by using sterile micropipette. The plates were then incubated in a BOD (Bio-Oxygen Demand) incubator at 37 °C for 48 h. The zone of inhibition (ZI) of each bacterial strain was measured in triplicate by using a calibrated digital Vernier caliper.

2.8.3. Broth microdilution method - MIC

MICs (Minimum Inhibitory Concentration) of the extracts, fractions and compounds against the bacterial and yeast strains and samples were determined using the microdilution method in 96 well plates (Cellstar®, Greinerbio-one, Germany) (Apaza et al., 2020). The MHB (Mueller--Hinton broth) medium (180 μL) of the bacterial culture and the Sabouraud medium (yeast culture) were used to fill the first experimental well. The other wells were filled with 100 μL of medium. Subsequently, a volume of 20 μL of (extracts, fractions and compounds) was added to the first well. Double fold serial dilution was then carried out across the plate. Overnight batch culture of the microorganisms (10 μL) was used to inoculate each well to achieve an inoculum size of ca. 1×10^6 CFU (Colony-Forming Unit)/mL. The plates were incubated for 48 h at 37 °C. MICs were calculated according to Apaza et al. (2020). DMSO at the same tested concentration was used as a negative control, while Ofloxacin (27.67 μM) was used as positive control to assess the accuracy of the MIC method. Each MIC determination was carried out in triplicate.

2.9. Statistical analysis

CC_{50} (Cytotoxic Concentration 50%) and IC_{50} (Inhibitory Concentration 50%) values were determined by non-linear regression. All the experiments were performed in triplicate. One-way ANOVA statistical analysis (Tukey's multiple comparisons test, $p < 0.05$; $p < 0.001$) was performed to evaluate the significant differences among values. All the analyses were performed using GraphPad Prism, version 8.4.0.

3. Results

3.1. Extraction, isolation and characterisation of compounds

In this report, we only include a detailed characterisation of compounds **1** and **3**, since they have not been previously reported as natural compounds. For compound **2**, only a brief characterisation has been included, because it has been widely described in numerous works as an isolated compound from different plant species (Fig. 1).

3.1.1. Characterisation of compound 1

4-[1-(3,5,5,8,8-Pentamethyl-5,6,7,8-tetrahydro-2-naphthalenyl)-vinyl]-benzoic acid or Bexarotene (**1**) was obtained as a white solid amorphous. Its molecular formula, $C_{24}H_{28}NaO_2$, was confirmed through HRESIMS $[M+Na]^+$ ion at m/z 371.2.

Nineteen signals were distinguished in the ^{13}C NMR spectrum, with seven signals between δ_C: 150-130 ppm corresponding to seven quaternary aromatic carbons. Likewise, between δ_C: 129-126 ppm, three signals correspond to five aromatic carbons (=CH-). The ^1H NMR spectrum showed ten signals differentiable into three systems of signals.

The first system is composed of two doublets of a proton which is coupled to the protons H-α (δ_H: 5.35 ppm, $J = 1.3$ Hz) and H-β (δ_H: 5.83 ppm, $J = 1.3$ Hz) of the vinyl substituent. Through the HSQC spectrum, it was confirmed that the H-α and H-β protons belong to the vinyl carbon (δ_C: 117.33 ppm). Likewise, through the HMBC spectrum, it was confirmed that the signals of the H-α and H-β protons are coupled with the α-vinyl carbon (δ_C: 149.28 ppm) and with the aromatic carbons C-2 (δ_C: 138.06 ppm) and C-1' (δ_C: 146.62 ppm).

Regarding the second benzyl system, it was observed that the protons H-5'/H-3' (δ_H: 8.07 ppm) are coupled with the equivalent protons H-6'/H-2' (δ_H: 7.41 ppm). Furthermore, from the HSQC and HMBC spectra, the H-5'/H-3′ protons correspond to the C-5'/C-3′ carbons (δ_C: 128.23 ppm). Likewise, the H-5'/H-3′ protons are coupled with the C-1′ carbons (δ_C: 146.62 ppm), carbonyl (δ_C: 171.10 ppm) and C-4' (δ_C: 130.45 ppm). Finally, the C-6'/C-2′ carbons (δ_C: 128.07 ppm) are coupled with the α-vinyl carbon (δ_C: 149.28 ppm).

Through the ^1H–^1H COSY, HSQC and HMBC spectra, we observed a methyl group in position 3 (δ_C: 20.09 ppm) in the third naphthenic system, with a singlet of three protons (δ_H: 1.95 ppm) which are coupled with the aromatic proton H-4 (δ_H: 7.08 ppm) (Fig. 2).

On the other hand, a methyl was observed in the position 3, which was coupled with the aromatic carbons C-3 (δ_C: 132.86 ppm), C-2 (δ_C:

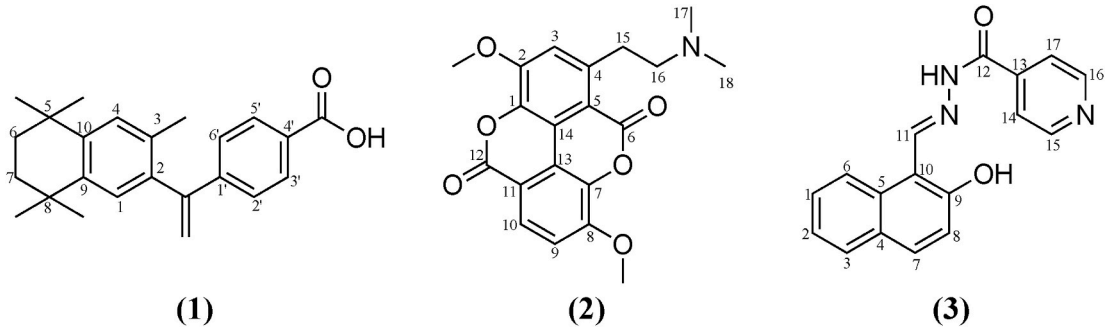

Fig. 1. The chemical structures of triterpenoids from *D. draco*. (**1**) Bexarotene; (**2**) Taspine; (**3**) 2-hydroxy-1-naphthaldehyde isonicotinoyl hydrazone.

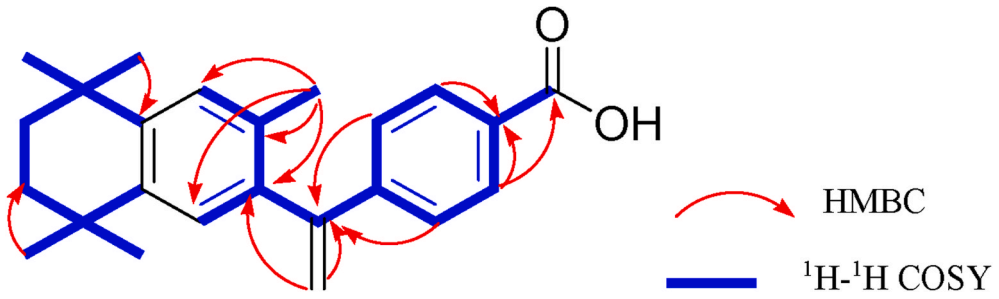

Fig. 2. Structural correlation of compound **1**.

138.06 ppm) and C-6'/C-2' (δ_C: 128.07 ppm). In addition, it was observed that carbon C-3 couples with the aromatic proton H-1 (δ_H: 7.13 ppm) and with the methyl protons in position 3.

Likewise, it was observed that the aromatic protons H-1 and H-4 are coupled with the C-8/C-5 carbons (δ_C: 35.35–35.37 ppm). A doublet of twelve protons was also observed at δ_H: 1.29 ppm, corresponding to four methoxy groups that are coupled with the C-7/C-6 carbons (δ_C: 34.16–34.06 ppm) and with the C-8/C-5 carbons. Finally, it was observed that the methyl groups at positions 12–15 and the C-6/C-7 carbons correlate with the C-9 (δ_C: 144.58 ppm) and C-10 (δ_C: 142.53 ppm) carbons.

3.1.2. Characterisation of compound 2

1-[2-(Dimethylamino)-ethyl]-3,8-dimethoxychromeno-[5,4,3-cde]-chromene-5,10-dione or Taspine (**2**) was obtained as an amorphous white solid; ^{1}H NMR (300 MHz, $CDCl_3$-d_1) δ_H: 8.13–8.11 (1H, d, H-10), 7.23 (1H, d, H-9), 7.12 (1H, s, H-3), 4.04 (6H, s, 2-OCH_3/8-OCH_3), 3.41 (2H, s, H-15'/H-15″), 2.57 (2H, m, H-16'/H-16″), 2.33 (6H, s, 17-CH_3/18-CH_3); ^{13}C NMR (76 MHz, $CDCl_3$-d_1) δ_C: 158.95 (C-12), 157.94 (C-6), 151.38–151.15 (C-2/C-8), 144.15 (C-7), 137.99–136.92 (C-1/C-4), 127.07 (C-10), 119.32 (C-14), 118.58 (C-13), 116.82 (C-3), 113.83 (C-11), 111.67 (C-9), 109.32 (C-5), 60.32 (C-16), 56.71–56.65 (2-OCH_3/8-OCH_3), 45.18 (C-17/C-18), 32.99 (C-15); $C_{20}H_{19}NO_6$. The spectroscopic data obtained for compound **2** were corroborated with the available literature references (Cheng et al., 2009; Altieri et al., 2013).

3.1.3. Characterisation of compound 3

N'-[(*E*)-(2-Hydroxy-1-naphthyl)-methylene]-isonicotinohydrazide or 2-hydroxy-1-naphthaldehyde isonicotinoyl hydrazone **(3)** was obtained as an amorphous white solid. Its molecular formula, $C_{17}H_{12}N_3O_2$, was confirmed through HRESIMS $[MH]^-$ ion at m/z 290.093.

The ^{13}C NMR spectrum showed that the imidolate carbon (C-12) appears at δ_C: 160.69 ppm, and the azomethine carbon (C-11) appears at δ_C: 151.34 ppm. The aromatic carbons, corresponding to the naphthenic ring and to isonicotynil ring, appeared between δ_C: 109–160 ppm. The ^{1}H NMR spectrum showed a one-proton singlet at δ_H: 9.58 ppm assigned to the allylic proton CH═N- (H-11). Next, two two-protons multiplets appeared at δ_H: 9.16–9.09 ppm and δ_H: 8.59–8.52 ppm that were assigned to the equivalent protons H-15/H-16 and H-14/H-17 of the isonycotynil ring. A correlation of the C-15/C-16 carbons (δ_C: 145.11 ppm) with the C-14/C-17 carbons (δ_C: 126.47 ppm) was observed through the HSQC spectrum. The correlations between the protons that make up the isonicotinyl ring, and between H-15/H-16 protons and the C-12 carbons (δ_C: 160.69 ppm) and C-13 (δ_C: 149.56 ppm) were observed through the HMBC spectrum.

We did not identify a resonance attributable to the N–H proton and the hydroxy group of the naphthenic ring in the ^{1}H NMR spectrum, revealing that we are witnessing a deprotonation. The protons of the naphthenic ring appear at δ_H: 8.2–7.2 ppm. Using ^{1}H–^{1}H COSY and HSQC spectra, the final structure was elucidated and the naphthenic protons H-6 (δ_H: 7.43 ppm, m), H-1 (δ_H: 7.60 ppm, m) and H-2 (δ_H: 8.25 ppm, d, $J = 8.5$ Hz) were correlated to the carbons C-6 (δ_C: 124.91 ppm), C-1 (δ_C: 129.03 ppm) and C-2 (δ_C: 121.34 ppm) (Fig. 3).

Using the HMBC spectrum, correlations between the proton H-11 and the carbons C-10 (δ_C: 109.29 ppm), C-5 (δ_C: 133.68 ppm) and C-9 (δ_C: 160.53 ppm) could be observed. In addition, the presence of C-9 in a weaker field indicates that the naphthenic ring is substituted in the ortho-position by a hydroxy group.

Finally, the complete elucidation was performed assigning the protons H-7 (δ_H: 7.95 ppm, d, $J = 9.0$ Hz), H-8 (δ_H: 7.24 ppm, dd, $J = 14.9$, 8.9 Hz) and H-3 (δ_H: 7.88 ppm, dd, $J = 8.2$, 1.4 Hz) to the carbons C-7 (δ_C: 134.14 ppm), C-8 (δ_C: 119.99 ppm) and C-3 (δ_C: 129.82 ppm).

3.2. Cytotoxic activity of the extracts

Regarding the cytotoxicity of the *D. draco* extracts, the results showed that the aqueous (CC_{50} = 91.20–96.60 μg/mL), dichloromethane (CC_{50} = 87.30–85.40 μg/mL) and alkaloid-rich dichloromethane (CC_{50} = 84.70–85.80 μg/mL) extracts did not show relevant cytotoxicity ($p = 0.074$) when compared to the positive control (Actinomycin D, CC_{50} = 7.95 *n*M) in any of the cell lines (THP-1, NIH-3T3 and HaCaT) (Table 1).

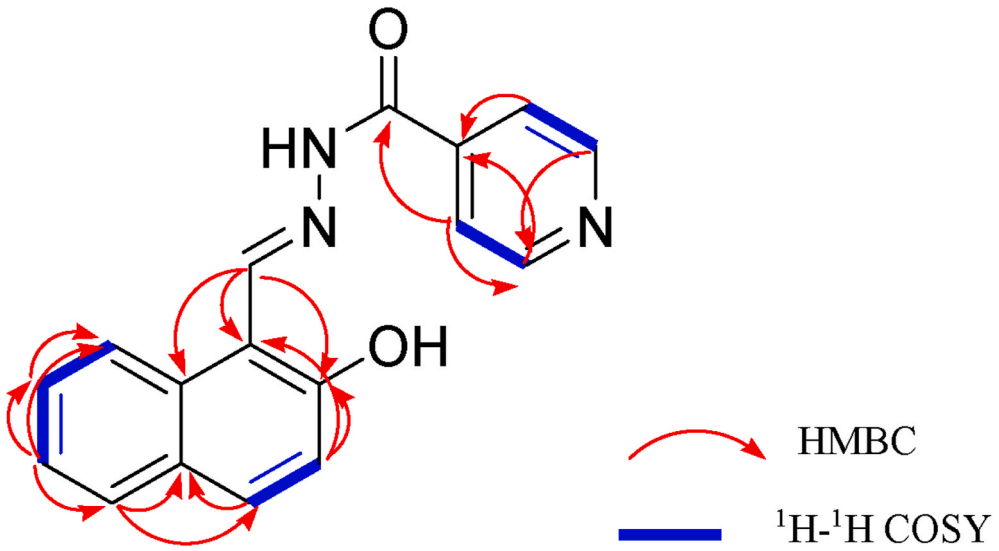

Fig. 3. Structural correlation of compound **3**.

Table 1
CC_{50s} of the LDH (Cytotoxicity) assays calculated for the extracts from *D. draco* CC_{50} was calculated using Prism v8.4.0 (GraphPad Software) using non-linear regression, dose-response curves. CI95%: Confidence interval 95%/Tukey's multiple comparisons test ($p < 0.001$***).

Extracts	Cytotoxicity (CC_{50} μg/mL) at 48 h (CI95%, R2)		
	THP-1	HaCaT	NIH-3T3
Untreated cells	98.26 (93.43–103.65, 0.9868)	99.37 (94.13–104.40, 0.9868)	98.49 (93.40–103.45, 0.9868)
DMSO	20.29 (15.94–25.91, 0.9615)	20.09 (15.56–24.59, 0.9615)	20.05 (15.41–25.11, 0.9615)
Actinomycin D[a]	7.97 (2.24–11.35, 0.9697)	7.95 (2.27–12.42, 0.9697)	7.92 (2.54–12.74, 0.9697)
HEX	75.00 (70.94–80.54, 0.9842)	73.30 (68.93–78.91, 0.9842)	73.05 (68.45–78.75, 0.9842)
DCM	87.30 (82.65 to 92.26, 0.9827)	86.50 (81.59 to 91.63, 0.9827)	85.40 (80.45 to 90.49, 0.9827)
MeOH	54.00 (49.71–59.62, 0.9824)	53.30 (48.90–58.06, 0.9824)	52.20 (47.88–57.84, 0.9824)
Aq	96.60 (91.62 to 101.99, 0.9979)	96.20 (91.39 to 101.76, 0.9979)	91.20 (86.65 to 96.64, 0.9979)
DCM-ALK	85.80 (80.49 to 90.98, 0.9851)	85.31 (80.17 to 90.86, 0.9851)	84.70 (79.82 to 89.06, 0.9851)

[a] Actinomycin D (CC_{50} = *n*M).

3.3. Anti-inflammatory activities of the extracts

Concerning the anti-inflammatory capacity, the results showed that the dichloromethane (IC_{50} = 60.80–58.90 μg/mL) and alkaloid-rich dichloromethane (IC_{50} = 64.10–65.69 μg/mL) extracts presented a greater inhibitory activity of the production of NF-κB than the aqueous extract (IC_{50} = 91.35–93.79 μg/mL) in all cell lines (Table 2).

On the other hand, the results concerning the activation of the Nrf2 factor confirmed that the dichloromethane (EC_{50} = 22.53–24.75 μg/mL) and alkaloid-rich dichloromethane (EC_{50} = 25.84–28.95 μg/mL) extracts presented statistically significant lower EC_{50} values ($p < 0.001$) than the aqueous extract (EC_{50} = 63.70–68.82 μg/mL) in all cell lines (Table 3).

Table 2
IC_{50s} of the inhibition of NF-κB production, calculated for the extracts from *D. draco*. IC_{50} was calculated using Prism v8.4.0 (GraphPad Software) using non-linear regression, dose-response curves. CI95%: Confidence interval 95%/Tukey's multiple comparisons test ($p < 0.001$***).

Extracts	Inhibition of NF-κB production (IC_{50} μg/mL) at 48 h (CI95%, R2)		
	THP-1	HaCaT	NIH-3T3
Untreated cells	19.98 (14.41–24.78, 0.9886)	17.24 (12.92–22.61, 0.9886)	16.46 (11.36–21.13, 0.9886)
Celastrol[a]	7.44 (2.72–11.33, 0.9891)	7.41 (2.43–12.90, 0.9891)	7.40 (2.76–12.40, 0.9891)
HEX	85.61 (80.27–90.72, 0.9568)	83.94 (78.13–88.77, 0.9568)	81.81 (76.24–86.93, 0.9568)
DCM	60.80 (55.13 to 65.11, 0.9856)	60.52 (55.73 to 65.61, 0.9856)	58.90 (53.95 to 63.95, 0.9856)
MeOH	49.93 (44.40–54.63, 0.9512)	46.33 (41.53–51.99, 0.9512)	46.26 (41.32–51.43, 0.9512)
Aq	93.79 (88.85–98.84, 0.9615)	93.71 (88.72–98.22, 0.9979)	91.35 (86.43–96.53, 0.9979)
DCM-ALK	65.69 (60.19 to 70.40, 0.9863)	65.06 (60.28 to 70.82, 0.9863)	64.10 (59.93 to 69.73, 0.9863)

[a] Celastrol (IC_{50} = μM).

3.4. Antimicrobial activities of the extracts

Regarding the antimicrobial capacity, the dichloromethane and alkaloid-rich dichloromethane extracts showed a statistically significant ZI ($p < 0.001$) on the *E. coli*, *C. albicans* and *S. aureus* type strains, with an IC_{50} of 27.19–29.37 μg/mL and 21.23–24.47 μg/mL, respectively (Table 4).

These results were confirmed by the MIC assay, where the extracts showed a MIC of 24.04–26.75 μg/mL (dichloromethane extract) and 18.58–19.92 μg/mL (alkaloid-rich dichloromethane extract), presenting a similar activity to the positive control (Ofloxacin, IC_{50} = 10.00 μg/mL) (p = 0.023) (Table 5).

3.5. Pro-proliferative activity of the extracts

Finally, in relation to the pro-proliferative properties (cell proliferation of NIH-3T3 fibroblasts and HaCaT keratinocytes), the

Table 3
EC_{50s} of the activation of Nrf2 production, calculated for the extracts from *D. draco*. EC_{50} was calculated using Prism v8.4.0 (GraphPad Software) using non-linear regression, dose-response curves. CI95%: Confidence interval 95%/ Tukey's multiple comparisons test ($p < 0.001$***).

Extracts	Activation of Nrf2 production (EC_{50} μg/mL) at 48 h (CI95%, R2)		
	THP-1	HaCaT	NIH-3T3
Untreated cells	1.96 (−4.54 to 6.52, 0.9973)	1.95 (−4.73 to 6.12, 0.9973)	1.89 (−4.43 to 6.94, 0.9973)
CDDO-Me[a]	0.11 (0.06–0.16, 0.9953)	0.11 (0.06–0.16, 0.9953)	0.10 (0.05–0.15, 0.9953)
HEX	57.01 (52.52–62.40, 0.9609)	56.41 (51.77–61.18, 0.9609)	53.98 (48.63–58.38, 0.9609)
DCM	24.75 (19.90 to 29.85, 0.9987)	22.53 (17.38 to 27.27, 0.9987)	22.12 (17.98 to 27.68, 0.9987)
MeOH	17.69 (12.49–22.48, 0.9781)	12.94 (7.90–17.81, 0.9781)	10.47 (5.28–15.09, 0.9781)
Aq	68.82 (63.93–73.24, 0.9873)	67.65 (62.06–72.85, 0.9873)	63.70 (58.14–68.89, 0.9873)
DCM-ALK	28.95 (23.44 to 33.61, 0.9968)	26.58 (21.53 to 31.77, 0.9968)	25.84 (20.50 to 30.71, 0.9968)

[a] CDDO-Me (IC_{50} = *n*M).

Table 4
In vitro culture plates (agar cup plate method) of *D. draco* extracts showing the zone of inhibition (ZI) concentration against different strains of microorganisms. IC_{50s} of the ZI was calculated using Prism v8.4.0 (GraphPad Software) using non-linear regression, dose-response curves. CI95%: Confidence interval 95%/ Tukey's multiple comparisons test ($p < 0.001$***).

Extracts	Zone of inhibition at (IC_{50} μg/mL) at 48 h (CI95%, R2)		
	S. aureus	*E. coli*	C. albicans
Ofloxacin[a]	27.65 (22.37–32.11, 0.9941)	27.67 (22.28–32.09, 0.9941)	27.71 (22.28–32.94, 0.9941)
HEX	93.56 (88.02–98.56, 0.9816)	94.19 (89.11–99.98, 0.9816)	96.39 (91.99–101.40, 0.9816)
DCM	27.19 (22.69 to 32.34, 0.9925)	27.41 (22.63 to 32.35, 0.9925)	29.37 (24.38 to 34.87, 0.9925)
MeOH	54.67 (49.53–59.51, 0.9847)	55.61 (50.38–60.42, 0.9847)	56.22 (51.75–61.32, 0.9847)
Aq	89.92 (84.84–94.45, 0.9869)	86.78 (81.08–91.34, 0.9869)	88.14 (83.70–93.65, 0.9869)
DCM-ALK	21.23 (16.51 to 26.65, 0.9928)	22.57 (17.90 to 27.97, 0.9928)	24.47 (19.58 to 29.30, 0.9928)

[a] Ofloxacin (IC_{50} = μM).

dichloromethane (IC_{50} = 36.43–37.16 μg/mL) and alkaloid-rich dichloromethane (IC_{50} = 30.39–34.65 μg/mL) extracts showed a higher pro-proliferative activity when compared to the other extracts (Fig. 4).

Given that the dichloromethane and alkaloid-rich dichloromethane extracts had greater pharmacological potential, they were selected for further fractionation.

3.6. Cytotoxic activity of the fractions

The dichloromethane extract was fractionated using DCM/MeOH as the mobile phase, producing eleven fractions that were subjected to cytotoxicity, anti-inflammatory and antimicrobial assays. Table 1S shows the cytotoxicity results; first fractions showed low cytotoxicity while the last fractions were highly cytotoxic, and the **F2** fraction (CC_{50} = 75.03–77.68 μg/mL) had the lowest cytotoxicity. **F2** had also statistically significant lower cytotoxicity than the other fractions.

The alkaloid-rich dichloromethane extract obtained through the liquid-liquid extraction technique was fractionated by column chromatography using the HEX, dioxane and MeOH solvents. Three fractions (1–3) were obtained. **F1'** and **F2'** had CC_{50} values between 71.56 and 76.32 μg/mL and 72.75–79.54 μg/mL, values which show a statistically significant lower cytotoxicity than the **F3**' (Table 6S).

Table 5
Minimum inhibitory concentration (MIC) of *D. draco* extracts against different strains of microorganisms. MIC was calculated using Prism v8.4.0 (GraphPad Software) using non-linear regression, dose-response curves. CI95%: Confidence interval 95%/Tukey's multiple comparisons test ($p < 0.001$***).

Extracts	Minimum inhibitory concentration at (MIC μg/mL) at 48 h (CI95%, R2)		
	S. aureus	*E. coli*	C. albicans
Ofloxacin[a]	27.65 (22.48–32.28, 0.9992)	27.67 (22.28–32.85, 0.9992)	27.71 (22.91–32.83, 0.9992)
HEX	87.33 (82.22–92.39, 0.9958)	89.71 (84.78–94.68, 0.9958)	91.24 (86.05–96.18, 0.9958)
DCM	24.04 (19.99 to 29.30, 0.9927)	25.49 (20.24 to 30.66, 0.9927)	26.75 (21.46 to 31.56, 0.9927)
MeOH	48.78 (43.57–53.85, 0.9908)	52.85 (47.72–57.07, 0.9908)	53.88 (48.52–58.80, 0.9908)
Aq	81.64 (76.99–86.25, 0.9944)	83.62 (78.82–88.04, 0.9944)	86.36 (81.84–91.73, 0.9944)
DCM-ALK	18.58 (13.92 to 23.39, 0.9924)	19.42 (14.05 to 24.05, 0.9924)	19.92 (14.61 to 24.32, 0.9924)

[a] Ofloxacin (IC_{50} = μM).

3.7. Anti-inflammatory activities of the fractions

The anti-inflammatory results showed that the **F2** fraction (IC_{50} = 44.40–44.70 μg/mL) has the highest inhibitory activity of the NF-κB production (Table 2S). Additionally, the results on the activation of the Nrf2 factor confirmed that the **F2** fraction (EC_{50} = 13.20–14.90 μg/mL) has statistically significant lower EC_{50} values than the other fractions in all cell lines (Table 3S).

Concerning the anti-inflammatory capacity of the fractions obtained from the alkaloid-rich dichloromethane extract, the results showed that the **F1'** (IC_{50} = 38.51–39.52 μg/mL) and **F2'** (IC_{50} = 32.95–35.09 μg/mL) fractions had a higher inhibitory activity of the NF-κB production than the **F3'** fraction (IC_{50} = 51.15–57.78 μg/mL) in all cell lines (Table 7S). Moreover, the results on the activation of the Nrf2 factor showed that the **F1'** (EC_{50} = 6.13–6.27 μg/mL) and **F2'** (EC_{50} = 4.31–5.63 μg/mL) fractions have statistically significant lower EC_{50} values than the **F3'** fraction (EC_{50} = 15.68–19.82 μg/mL) in all cell lines (Table 8S).

3.8. Antimicrobial activities of the fractions

The **F2** fraction showed a statistically significant ZI, with an IC_{50} of 11.51–13.61 μg/mL (Table 4S). This result was confirmed by the MIC assay, where the **F2** fraction showed a MIC of 8.40–9.49 μg/mL, having an antimicrobial activity similar to the positive control (Ofloxacin, IC_{50} = 10.00 μg/mL) (p = 0.095) (Table 5S).

Fractions **F1'** and **F2'** showed a statistically significant ZI, with an IC_{50} of 3.99–5.48 μg/mL and 2.36–3.17 μg/mL (Table 9S). These results were confirmed by the MIC assay, where the fractions showed a MIC of 2.03–2.91 μg/mL (**F1'**) and 1.66–1.96 μg/mL (**F2'**). Both fractions have a higher activity than the positive control (Ofloxacin, IC_{50} = 10.00 μg/mL) ($p < 0.001$) (Table 10S).

Through the chromatographic separation of the **F2** fraction, a total of eight fractions (F2.I–F2. VIII) were obtained, with **F2.VIII** (**Bexarotene**) as the most active fraction (Tables 11S–15S). Likewise, the chromatographic purification of the fractions **F1'-F2'** led to obtaining **Taspine** and **2-hydroxy-1-naphthaldehyde isonicotinoyl hydrazone**, which were the most active fractions.

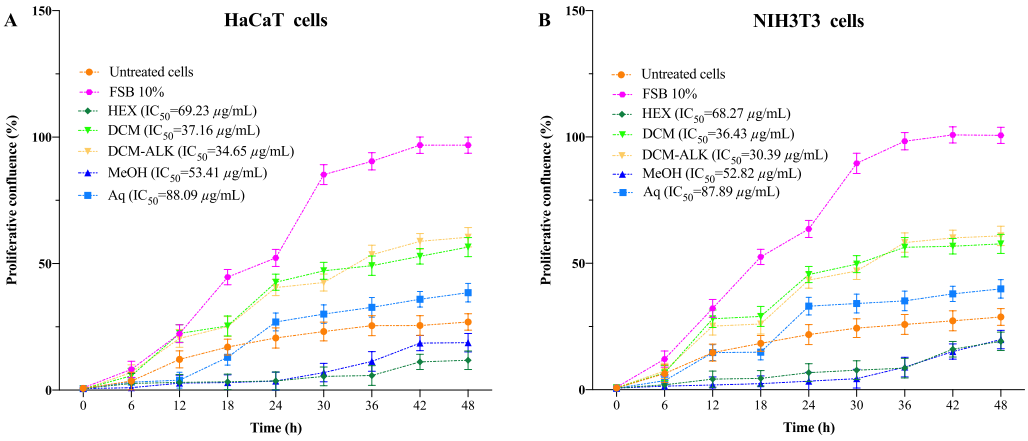

Fig. 4. Effect of extracts from *D. draco* on pro-proliferative activity in HaCaT (**A**) and NIH3T3 (**B**) cells.

3.9. Cytotoxic activity of the compounds

Table 6 shows the cytotoxicity of the pure compounds. **Bexarotene** (compound **1**, CC_{50} = 87.12–87.95 μM) had lower cytotoxicity than compounds **2-hydroxy-1-naphthaldehyde isonicotinoyl hydrazone** (compound **3**, CC_{50} = 71.58–75.41 μM) and **Taspine** (compound **2**, CC_{50} = 66.77–69.31 μM).

3.10. Anti-inflammatory activities of the compounds

The three compounds showed an inhibitory capacity of the NF-κB production higher than the positive control (Celastrol, IC_{50} = 7.43 μM), with IC_{50} values of 0.10–0.13 μM (compound **1**), 0.22–0.24 μM (compound **2**) and 3.75–4.78 μM (compound **3**) (Fig. 5).

Moreover, regarding the stimulation of Nrf2, effective concentrations of 5.34–5.43 *n*M (compound **1**), 163.20–169.20 *n*M (compound **2**) and 300.82–315.56 *n*M (compound **3**) were obtained. There are no previous reports on the effect of these three compounds on the production of Nrf2. However, although the isolated compounds showed Nrf2 stimulating activity, they are not better than the positive control (CDDO-Me, IC_{50} = 0.11 *n*M). Compound **1** is the one that has the highest Nrf2 stimulation potential, and as such is the one that would be the closest to the values displayed by the positive control (Fig. 6).

Table 6
CC_{50s} of the LDH (cytotoxicity) assays calculated for the compounds from *D. draco*. CC_{50} was calculated using Prism v8.4.0 (GraphPad Software) using non-linear regression, dose-response curves. CI95%: Confidence interval 95%/ Tukey's multiple comparisons test ($p < 0.001$).

Samples	Cytotoxicity (CC_{50} μM) at 48 h (CI95%, R2)		
	THP-1	HaCaT	NIH-3T3
Untreated cells	99.78 (94.11–104.60, 0.9807)	98.96 (93.39–103.83, 0.9807)	98.98 (93.75–103.71, 0.9807)
DMSO	20.34 (15.23–25.45, 0.9819)	20.34 (15.70–24.62, 0.9819)	20.12 (15.18–25.59, 0.9819)
Actinomycin D[a]	7.96 (2.76–12.43, 0.9924)	7.95 (2.56–11.94, 0.9924)	7.95 (2.28–12.04, 0.9924)
Compound 1	87.95 (82.04–92.15, 0.9913)	87.61 (82.66–92.79, 0.9913)	87.12 (82.85–92.11, 0.9913)
Compound 2	69.31 (64.31–74.49, 0.9958)	67.55 (62.06–72.84, 0.9958)	66.77 (61.25–71.61, 0.9958)
Compound 3	75.41 (70.44–80.12, 0.9951)	74.27 (69.57–79.22, 0.9951)	71.58 (66.07–76.35, 0.9951)

[a] Actinomycin D (CC_{50} = *n*M).

3.11. Pro-proliferative activity of the compounds

It was observed that compound **1** (IC_{50} = 8.62–8.71 *n*M) had a higher pro-proliferative activity, similar to the positive control (FSB, 100%). Compounds **2** (IC_{50} = 166–171 *n*M) and **3** (IC_{50} = 469–486 *n*M) showed a pro-proliferative activity of 75% and 65% (Fig. 7).

3.12. Antimicrobial activities of the compounds

The three compounds showed a statistically significant ZI in the *E. coli*, *C. albicans* and *S. aureus* strains, with an IC_{50} of 0.14–0.19, 0.41–0.49 and 4.69–4.86 μM, respectively (Fig. 8). The ZI of compound **1** was higher than that of Ofloxacin (positive control).

These results were corroborated through the minimum inhibitory concentration (MIC) assay, obtaining MIC values of 0.12–0.16 μM (compound **1**), 0.31–0.39 μM (compound **2**) and 3.96–3.99 μM (compound **3**). Thus, the compounds showed higher antimicrobial activity than the positive control (Ofloxacin, IC_{50} = 27.67 μM) (Fig. 9).

4. Discussion

The three isolated compounds have been described in previous works. However, this is the first time they have been isolated in the *D. draco* species. In this sense, compound **1** was first synthesised in 1993 by Ligand Pharmaceuticals Inc. (Boehm et al., 1993). In relation to compound **2**, it has been isolated from different plant species such as: *Leontice eversmannii* (Platonova et al., 1953), *Croton Lechleiri* (Perdue et al., 1979) and *Magnolia liliflora* (Talapatra et al., 1982). Finally, in relation to compound **3**, it was synthesised for the first time by Sacconi (1953).

There are no studies regarding the cytotoxicity of *D. draco* extracts. However, there is a toxicity study that reported that the ethyl acetate extract from *D. draco* did not show toxicity at a dose of 8000 mg/kg body weight (lethal dose 50) in Sprague Dawley rats. Macroscopic observation of the liver and kidneys showed that there were no abnormalities and that the organ weights were within normal values (Yunita and Mursyid, 2019). Relating the toxicity data obtained from previous work and the cytotoxicity results obtained in our work, we can conclude that there is a relationship between cytotoxicity/toxicity and the polarity of the extracts. In this sense, the apolar extracts showed greater cytotoxicity/toxicity than the polar extracts.

Regarding the compounds isolated from the dichloromethane and alkaloid-rich dichloromethane extracts, previous studies have shown that compound **1** was not cytotoxic in the PC12 cell lines (CC_{50} > 100 μM) (Wang et al., 2019); in our study we confirmed that this compound

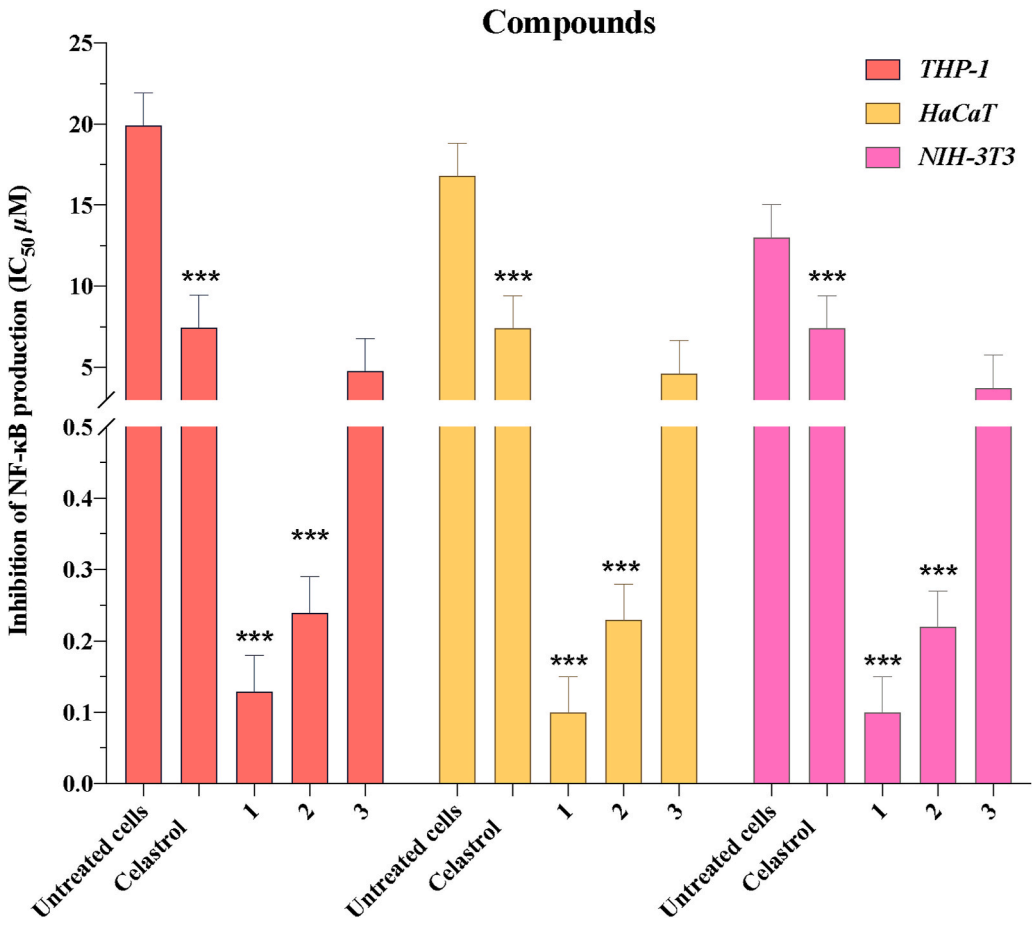

Fig. 5. IC_{50s} of the inhibition of NF-κB production, calculated for the compounds from *D. draco* at 48 h. IC_{50} was calculated using Prism v8.4.0 (GraphPad Software) using non-linear regression, dose-response curves. CI95%: Confidence interval 95%/Tukey's multiple comparisons test ($p < 0.001$).

was not cytotoxic in any of the cell lines. Compound **2** did not show relevant cytotoxicity confirming the results previously reported in KB tumour ($CC_{50} = 0.39$ μg/mL) and V-79 ($CC_{50} = 0.17$ μg/mL) cell lines by Itokawa et al. (1991). Finally, compound **3** has been reported as cytotoxic against different tumour cell lines confirming the results of Green et al. (2001) ($IC_{50} = 0.65–2.3$ μM). Our study shows that the compound **3** is not cytotoxic. This contradiction between our results and those reported in previous reports may be because the tests were conducted in different cell lines, with different morphological features.

On the other hand, in relation to the anti-inflammatory activity of the extracts of *D. draco*, previous studies have shown that the ethanolic extract of *D. draco* presented anti-inflammatory activity (inhibition of the production of interleukin 1β, TNF-α and NF-κB) in a range of concentrations between 10 and 200 μg/mL (Choy et al., 2008). Furthermore, the ethanolic extract of *D. draco* stimulated the production of HO-1 (Heme Oxygenase 1) which is directly related to the suppression of NF-κB and to the activation of Nrf2 (Wardyn et al., 2015). This potential was confirmed in our case through the methanolic extract that presented an inhibitory activity of NF-κB (IC_{50} = 46.26–49.39 μg/mL) and a stimulating activity of Nrf2 ($IC_{50} = 10.47–17.69$ μg/mL). However, this extract was not studied due to its cytotoxicity (CC_{50} = 52.20–54.00 μg/mL).

Regarding the anti-inflammatory activity of the compounds, previous studies have reported the inhibition potential over the NF-κB production of compound **1**, inhibiting the phosphorylation of Iκβα in chondriosomes (Zha et al., 2020). Concerning compounds **2** and **3**, there are no reports on their effect on the production of NF-κB. However, there are reports that mention that compound **2** has anti-inflammatory activity (Perdue et al., 1979; Raintree Nutrition, 2007) and compound **3** attenuates ROS production (Wang et al., 2016).

The mechanism of action of compounds **2** and **3** on the NF-κB pathway is unknown. However, our results show that these compounds are better than the positive control (Celastrol). If we account for the fact that the mechanism of action of Celastrol is through the suppression of the degradation of Iκβα and inhibition of the translocation of p65 of the nucleus (Youn et al., 2014), we can deduct that compounds **2** and **3** act on these factors on the NF-κB inhibition pathway.

On the other hand, analysing the mechanism of action of the positive control (CDDO-Me) on the Nrf2 pathway, we observe that it acts by generating bonds with the thiol groups of the Keap-1 unit, which leads to the release of the Nrf2 unit. This release leads to subsequent nuclear transcription and the production of a coordinated antioxidant and anti-inflammatory response (Wang et al., 2014). Based on this premise, a similar mechanism of action on the Nrf2 pathway can be assumed for the three compounds.

Additionally, the anti-inflammatory activity of the compounds can be related to their lipophilic capacity. This concerns the partition coefficient of the three compounds. The higher the partition coefficient (Log P), the more hydrophobic the compound is and, therefore, it is better distributed in hydrophobic environments such as the lipid bilayers that make up cells (Kapustikova et al., 2018). Based on this premise, compound **1** is the most absorbable since it has a Log P of 6.86 (compound **2**, Log P of 3.18, and compound **3**, Log P of 2.18).

We can conclude that both the inhibition of the NF-κB nuclear factor and the activation of the Nrf2 factor are crucial for the anti-inflammatory action during the pro-proliferative process (Ahmed et al., 2017). The isolated compounds have shown both activities.

In relation to the antimicrobial activity of extracts of *D. draco*,

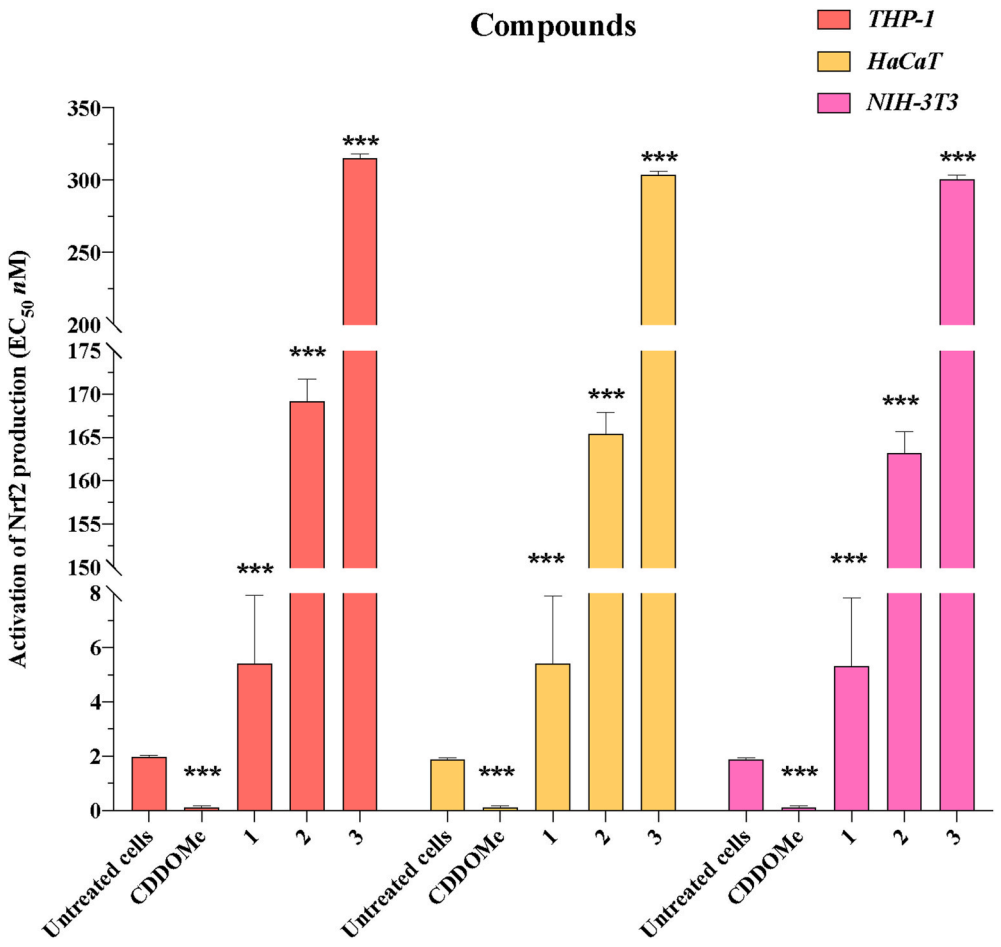

Fig. 6. EC_{50s} of the activation of Nrf2 production, calculated for the compounds from *D.* draco at 48 h. EC_{50} was calculated using Prism v8.4.0 (GraphPad Software) using non-linear regression, dose-response curves. CI95%: Confidence interval 95%/Tukey's multiple comparisons test ($p < 0.001$).

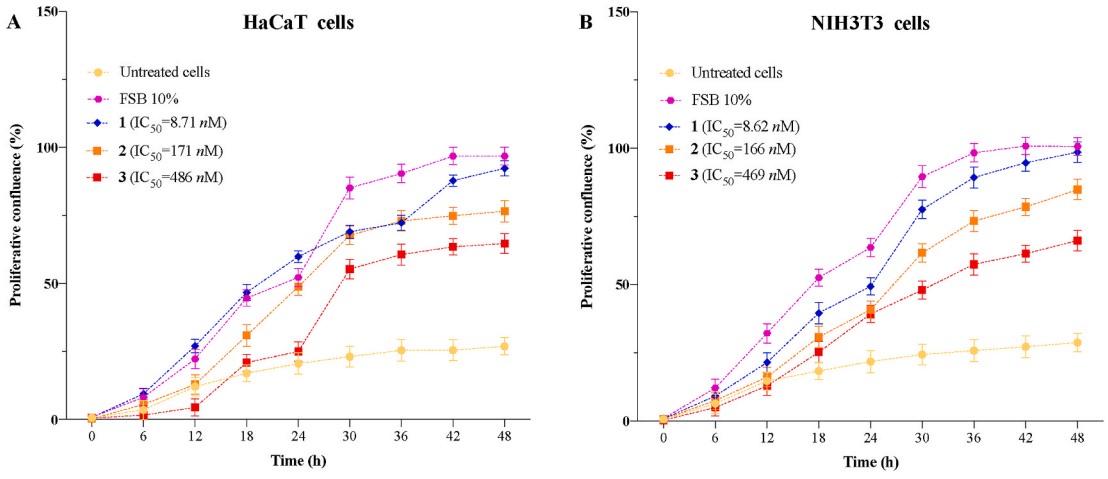

Fig. 7. Effect of compounds from *D. draco* on pro-proliferative activity in HaCaT (**A**) and NIH3T3 (**B**) cells.

Wahyuni et al. (2018) reported that hexane (ZI = 10.57 μg/mL), ethyl acetate (ZI = 15.05 μg/mL, MIC = 1.0 mg/mL) and methanol (ZI = 13.40 μg/mL, MIC = 0.5 mg/mL) extracts of *D. draco* have antimicrobial activity against *S. aureus*. Our study shows that the hexane and methanolic extracts have ZI of 96.56 μg/mL and 54.67 μg/mL against the *S. aureus* strain, with MIC results of 87.33 and 48.78 μg/mL, respectively. Furthermore, these extracts showed similar activities against *E. coli* and *C. albicans* strains. Thus, our results confirm the activity of *D. draco* extracts on Gram-positive bacteria (*S. aureus*). Moreover, our study highlights the antimicrobial activity on Gram-negative bacteria (*E. coli*) and yeasts (*C. albicans*).

Regarding the antimicrobial activity of the compounds, there are previous studies on the antimicrobial activity of compound **1** against Gram-positive bacteria (*P. acnes*) (Aranegui and García-Cruz, 2012). There are no previous reports of the antimicrobial activity of compound **2**. Concerning compound **3**, its antimicrobial activity was reported

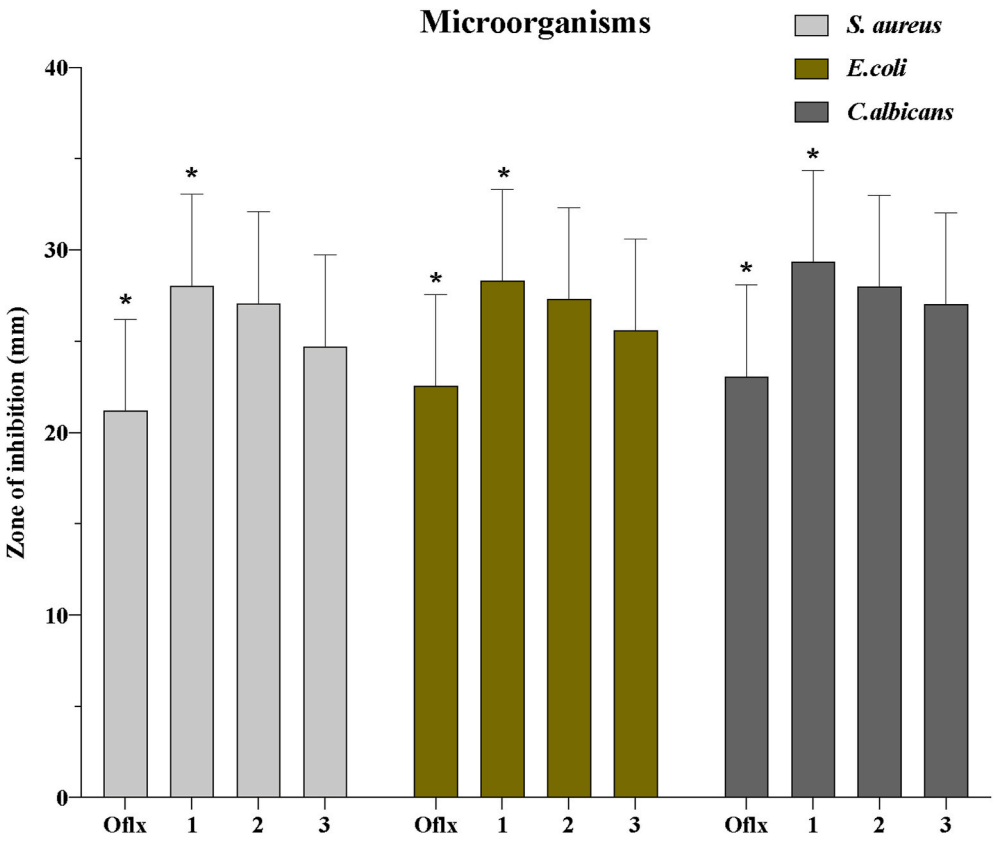

Fig. 8. *In vitro* culture plates (agar cup plate method) of *D. draco* compounds showing the zone of inhibition (ZI) concentration against different strains of microorganisms at 48 h IC_{50s} of the ZI was calculated using Prism v8.4.0 (GraphPad Software) using non-linear regression, dose-response curves. CI95%: Confidence interval 95%/Tukey's multiple comparisons test ($p < 0.001$).

against *S. aureus* (Gram-positive), *E. coli* (Gram-negative) and *C albicans* (yeast), with an inhibitory concentration of 2.07, 2.07 and 2.37 μM, respectively (Judge et al., 2011). These results are similar to those obtained in the current report.

Analysing the mechanism of antimicrobial action of Ofloxacin, we observed that it inhibits topoisomerases II, IV and DNA gyrase that are necessary to complete the cycle of bacterial division (Todd and Faulds, 1991). In this sense, our compounds can have a similar mechanism of action, however this should be further analysed in future studies.

Finally, we observed that the pro-proliferative activity of compound **1** is due to its retinoid type structure; compound **1** produces an increase of fibroplasia and angiogenesis (Fernández and Armario, 2003). In relation to compound **2**, there are reports on its pro-proliferative activity in the early stages of the wound. This is because it promotes the migration of fibroblasts at 50 *pg*/mL (Porras-Reyes et al., 1993). However, compound **2** has been shown to have a higher pro-proliferative activity in its salt form (De Fátima et al., 2008). Furthermore, *in vitro* assays have shown that, after its application, compound **2** produces an acceleration in the growth of collagen, capillaries (angiogenesis), as well as an increase in the autocrine of TGF-β, and the EGF (Epidermal Growth Factor) in fibroblasts (Raintree Nutrition, 2007). Concerning compound **3**, Walcourt et al. (2013) showed that it is an iron chelator. Iron chelators are used as pharmacological agents because they suppress the lack of iron, accelerating the pro-proliferative process (Wright et al., 2014).

In vitro studies (cell cultures) provided us with information on the possible mechanism of anti-inflammatory and pro-proliferative activities of the extracts, fractions and compounds isolated from *Daemonorops draco* (Willd.) Blume species. However, to support the idea of action on NF-κB (suppression of phosphorylation of IKKαβ) and pro-proliferative activity, it would be beneficial to perform *in vivo* and mechanistic studies.

5. Conclusion

This report has confirmed the anti-inflammatory, pro-proliferative and antimicrobial activities of the *D. draco* resin. Moreover, this study is the first report isolating Bexarotene (**1**), Taspine (**2**) and 2-hydroxy-1-naphthaldehyde isonicotinoyl hydrazone (**3**) from the *Daemonorops draco* (Willd.) Blume species. For compounds **1** and **3**, it is the first time that they have been isolated from a natural product, given that previous authors have only obtained these compounds through chemical synthesis. Although compound **2** has been considered a biomarker of the *Croton lechleri* species, this work confirms its presence in the *D. draco* species. The chemical relation between these species and other "Dragon's blood" species should be analysed in future studies.

The current report has shown that the three compounds could be used to develop topical treatments seen as healing alternatives to those already on the market. In addition, future reports on these compounds could use them for unveiling the relation between structure and activity (SAR). In addition to these three compounds, bio-guided isolation should look for new compounds since the *D. draco* species has not been comprehensively studied, and our study is only a first step towards such efforts.

Author contributions

S.S.C.J and A.T.L performed the phytochemical analysis and isolation of compounds. O.D.M performed biological experiments and helped with the manuscript writing and figures preparation. I.M.P. helped with the statistical analysis of the data. R.S.A conceived and supervised the study, provided the plant materials and helped with the manuscript writing. A.T.L. conceived and supervised the study, performed the experiments and the statistical analysis and wrote and edited the

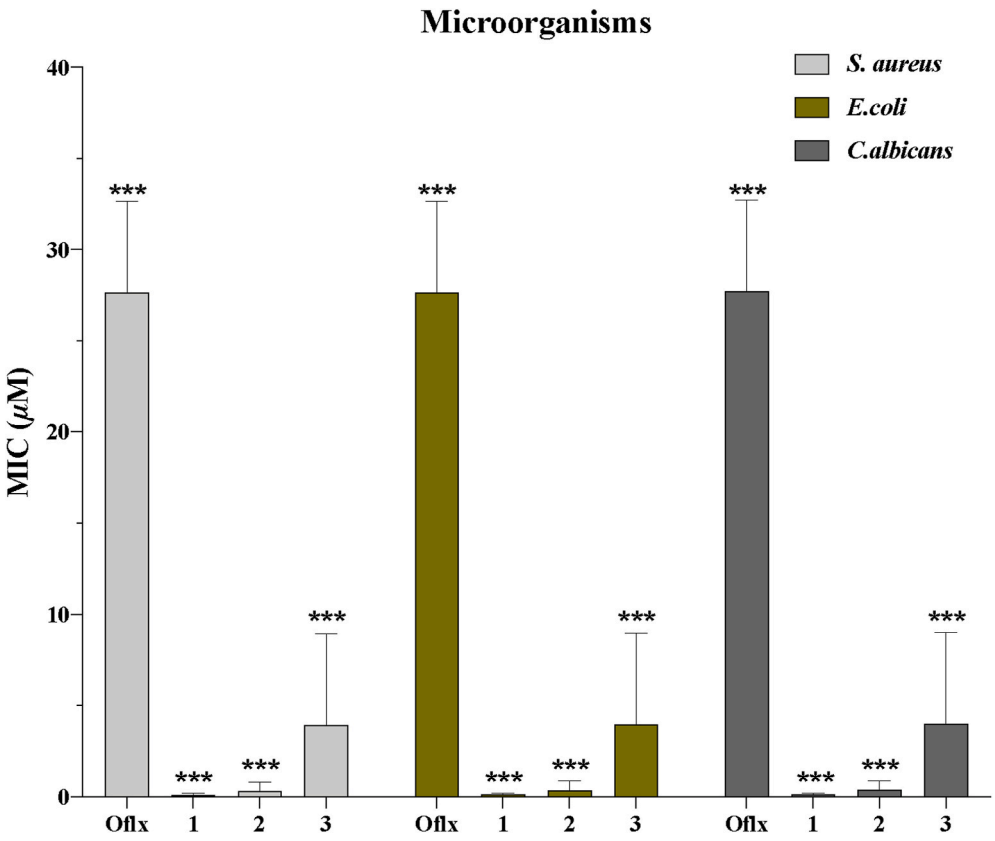

Fig. 9. Minimum inhibitory concentration (MIC) of *D. draco* compounds against different strains of microorganisms at 48 h. MIC was calculated using Prism v8.4.0 (GraphPad Software) using non-linear regression, dose-response curves. CI95%: Confidence interval 95%/Tukey's multiple comparisons test ($p < 0.001$).

manuscript and the figures. All authors read and approved the final manuscript.

Declaration of competing interest

The authors declare no conflict of interest.

Acknowledgments

This work was supported by the National Herbarium of Bolivia, the Fundación de la Universidad Autónoma de Madrid (FUAM).

Appendix A. Supplementary data

Supplementary data to this article can be found online at https://doi.org/10.1016/j.jep.2020.113668.

References

Agyare, C., Akindele, A.J., Steenkamp, V., 2019. Natural products and/or isolated compounds on wound healing. Evid Based Complement Alternat Med 2019, 4594965. https://doi.org/10.1155/2019/4594965.

Ahmed, S.M., Luo, L., Namani, A., Wang, X.J., Tang, X., 2017. Nrf2 signaling pathway: pivotal roles in inflammation. Biochim. Biophys. Acta (BBA) - Mol. Basis Dis. 1863 (2), 585–597. https://doi.org/10.1016/j.bbadis.2016.11.005.

Altieri, A., Franceschin, M., Nocioni, D., Alvino, A., Casagrande, V., Scarpati, L., Bianco, A., 2013. Total synthesis of taspine and a symmetrical Analogue : study of binding to G-quadruplex DNA by ESI-MS. Eur. J. Org Chem. 191–196 https://doi.org/10.1002/ejoc.201201034.

Ambrozova, N., Ulrichova, J., Galandakova, A., 2017. Models for the study of skin wound healing. The role of Nrf2 and NF-κB. Biomed Pap Med Fac Univ Palacky Olomouc Czech Repub 161, 1–13. https://doi.org/10.5507/bp.2016.063.

Apaza, T.L., Rumbero, S.Á., Orosco, G.Ó., Ortega, D.M., 2020. Antimicrobial compounds isolated from *Tropaeolum tuberosum*. Nat. Prod. Res. 1–5 https://doi.org/10.1080/14786419.2019.1710700.

Aranegui, B., García-Cruz, A., 2012. Topical retinoids. In: Conde-Taboada, A. (Ed.), Dermatological Treatments, pp. 125–152. Madrid.

Ashrafi, M., Baguneid, M., Bayat, A., 2016. The role of neuro mediators and innervation in cutaneous wound healing. Acta Derm. Venereol. 96, 587–597. https://doi.org/10.2340/00015555-2321.

Boehm, M.F., Heyman, R.A., Zhi, L. (1993, October 22). USA Patent No. WO9321146..

Cavaillon, J.M., 2018. Exotoxins and endotoxins: inducers of inflammatory cytokines. Toxicon 149, 45–53. https://doi.org/10.1016/j.toxicon.2017.10.016.

Cheng, B., Zhang, S., Zhu, L., Zhang, J., Li, Q., Shan, A., He, L., 2009. Facile and Efficient Total Synthesis of Taspine. Synthesis (Stuttg), pp. 2501–2504. https://doi.org/10.1055/s-0029-1217393.

Choy, C.S., Hu, C.M., Chiu, W.T., Lam, C.S.K., Ting, Y., Shin-Han Tsai, S.H., Wang, T.C., 2008. Suppression of lipopolysaccharide-induced of inducible nitric oxide synthase and cyclooxygenase-2 by Sanguis Draconis, a dragon's blood resin, in RAW 264.7 cells. J. Ethnopharmacol. 115, 455–462. https://doi.org/10.1016/j.jep.2007.10.012.

De Fátima, A., Modolo, L.V., Andréia Sanches, A.C., Porto, R.R., 2008. Wound healing agents: the role of natural and non-natural products in drug development. Mini Rev. Med. Chem. 8, 879–888. https://doi.org/10.2174/138955708785132738.

Eichenfield, D.Z., Troutman, T.D., Link, V.M., Lam, M., Cho, H., Gosselin, D., Spann, N.J., Lesch, H.P., Tao, J., Muto, J., Gallo, R.L., Evans, R.M., Glass, C.K., 2016. Tissue damage drives co-localization of NF-κB, Smad 3, and Nrf2 to direct Rev-erb sensitive wound repair in mouse macrophages. Elife 5, e13024. https://doi.org/10.7554/eLife.13024.

Fazil, M., Nikhat, S., 2020. Topical medicines for wound healing: a systematic review of Unani literature with recent advances. J. Ethnopharmacol. 257, 112878. https://doi.org/10.1016/j.jep.2020.112878.

Fernández, J.M., Armario, J.C., 2003. Retinoides en dermatología. Med Cutan Iber Lat Am 31 (5), 271–294.

Georgescu, M., Marinas, O., Popa, M., Stan, T., Lazar, V., Bertesteanu, S.V., Chifiriuc, M. C., 2016. Natural compounds for wound healing. In: Fonseca C. Worldwide Wound Healing. https://doi.org/10.5772/65652.

Gonzalez, A.C., Costa, T.F., Andrade, Z.A., Medrado, A.R., 2016. Wound healing-A literature review. An. Bras. Dermatol. 91, 614–620. https://doi.org/10.1590/abd1806-4841.20164741.

Gottrup, F., Apelqvist, J., Bjarnsholt, T., Cooper, R., Moore, Z., Peters, E.J., Probst, S., 2013. EWMA document: antimicrobials and non-healing wounds. Evidence, controversies and suggestions. J. Wound Care 22, S1–S89. https://doi.org/10.12968/jowc.2013.22.Sup5.S1.

Green, D.A., Antholine, W.E., Wong, S.J., Richardson, D.R., Chitambar, C.R., 2001. Inhibition of malignant cell growth by 311, a novel iron chelator of the pyridoxal

isonicotinoyl hydrazone class: effect on the R2 subunit of ribonucleotide reductase. Clin. Canc. Res. 7 (11), 3574–3579.
Gupta, D., Bleakley, B., Gupta, R.K., 2007. Dragon's blood: botany, chemistry and therapeutic uses. J. Ethnopharmacol. 115, 361–380. https://doi.org/10.1016/j.jep.2007.10.018.
Hiebert, P., Werner, S., 2019. Regulation of wound healing by the nrf2 transcription factor-more than cytoprotection. Int. J. Mol. Sci. 20 https://doi.org/10.3390/ijms20163856.
Hop, H.T., Reyes, A.W.B., Huy, T.X.N., Arayan, L.T., Min, W.G., Lee, H.J., Rhee, M.H., Chang, H.H., Kim, S., 2017. Activation of NF-kB-Mediated TNF-induced antimicrobial immunity is required for the efficient Brucella abortus clearance in RAW 264.7 cells. Front Cell Infect Microbiol 7, 437. https://doi.org/10.3389/fcimb.2017.00437.
Hülpüsch, C., Tremmel, K., Hammel, G., Bhattacharyya, M., de Tomassi, A., Nussbaumer, T., Neumann, A.U., Reiger, M., Traidl-Hoffmann, C., 2020. Skin pH-dependent *Staphylococcus aureus* abundance as predictor for increasing atopic dermatitis severity. Allergy 75 (11), 2888–2898. https://doi.org/10.1111/all.14461, 10.1111/all.14461. Advance online publication.
Itokawa, H., Ichihara, Y., Mochizuki, M., Enomori, T., Morita, H., Shirota, O., Inamatsu, M., Takeya, K., 1991. A cytotoxic substance from sangre de Grado. Chem. Pharm. Bull. 39 (4), 1041–1042. https://doi.org/10.1248/cpb.39.1041.
Judge, V., Narasimhan, B., Ahuja, M., Sriram, D., Yogeeswari, P., De Clercq, E., Pannecouque, C., Balzarini, J., 2011. Isonicotinic acid hydrazide derivatives: synthesis, antimicrobial activity, and QSAR studies. Med. Chem. Res. 21, 1451–1470. https://doi.org/10.2174/157340613804488404.
Kabashima, K., Honda, T., Ginhour, F., Egawa, G., 2019. The immunological anatomy of the skin. Nat. Rev. Immunol. 19, 19–30. https://doi.org/10.1038/s41577-018-0084-5.
Kapustikova, I., Bak, A., Gonec, T., Kos, J., Kozik, V., Jampilek, J., 2018. Investigation of hydro-lipophilic properties of N-alkoxyphenylhydroxynaphthalenecarboxamides. Molecules 23, 1635. https://doi.org/10.3390/molecules23071635.
Kashem, S.W., Kaplan, D.H., 2016. Skin immunity to *Candida albicans*. Trends Immunol. 37 (7), 440–450. https://doi.org/10.1016/j.it.2016.04.007.
Kuo, P.C., Hung, H.Y., Hwang, T.L., Du, W.K., Ku, H.C., Lee, E.J., Tai, S.H., Chen, F.A., Wu, T.S., 2017. Anti-inflammatory flavan-3-ol-dihydroretrochalcones from *Daemonorops draco*. J. Nat. Prod. 80, 783–789. https://doi.org/10.1021/acs.jnatprod.7b00039.
Lawrence, T., 2009. The nuclear factor NF-kappaB pathway in inflammation. Cold Spring Harb Perspect Biol 1, a001651. https://doi.org/10.1101/cshperspect.a001651.
Merlini, L., Nasini, G., 1976. Constituents of dragon's blood. II. Structure and oxidative conversion of a novel secobiflavonoid. J. Chem. Soc. Perkin Trans. I 1, 1570. https://doi.org/10.1039/P19760001570.
Nasini, G., Piozzi, F., 1981. Pterocarpol and triterpenes from *Daemonorops draco*. Phytochemistry 20, 514–516. https://doi.org/10.1016/S0031-9422(00)84180-1.
Opal, S.M., DePalo, V.A., 2000. Anti-inflammatory cytokines. Chest 117, 1162–1172. https://doi.org/10.1378/chest.117.4.1162.
Perdue, G.P., Blomster, R.N., Blake, D.A., Farnsworth, N.R., 1979. South American plants 11: taspine isolation and anti-inflammatory activity. J. Pharmacol. Sci. 68 (1), 124–126. https://doi.org/10.1002/jps.2600680145.
Petkovsek, Z., Elersic, K., Gubina, M., Zgur-Bertok, D., Starcic Erjavec, M., 2009. Virulence potential of *Escherichia coli* isolates from skin and soft tissue infections. J. Clin. Microbiol. 47 (6), 1811–1817. https://doi.org/10.1128/JCM.01421-08.
Piozzi, F., Passannanti, S., Paternostro, M.P., Nasini, G., 1974. Diterpenoid resin acids of *Daemonorops draco*. Phytochemistry 13, 2231–2233. https://doi.org/10.1016/0031-9422(74)85033-8.
Platonova, T.F., Kuzovkov, A.D., Massagetov, P.S., 1953. Alkaloids of plants, Leontice eversmannii. I. New alkaloid taspine and alkaloid isoleontine. Preparation of leontidane and isoleontane. Russ. J. Gen. Chem. 23, 880–886.
Porras-Reyes, B.H., Lewis, W.H., Roman, J., Simchowitz, L., Mustoe, T.A., 1993. Enhancement of wound healing by the alkaloid taspine defining mechanism of action. Exp. Biol. Med. 203 (1), 18–25. https://doi.org/10.3181/00379727-203-43567.
Proksch, E., 2018. PH in nature, humans and skin. J. Dermatol. (Tokyo) 45, 1044–1052. https://doi.org/10.1111/1346-8138.14489.
Purwanti, S., Wahyuni, W.T., Batubara, I., 2019. Antioxidant activity of *Daemonorops draco* resin. J. Kim. Sains dan Apl. 22, 179. https://doi.org/10.14710/jksa.22.5.179-183.
Raintree Nutrition, I., 2007. Biological Activities for Sangre de Grado (*Croton lechleri*) [WWW Document]. URL. https://rain-tree.com/sangre-de-grado-activity.pdf. accessed 9.12.2020.
Sacconi, L., 1953. Chemical reactions leading to the formation of complexes. Polymeric polynuclear nickel complexes with hydrazides of β-pyridine- and γ-pyridinecarboxylic acids. Gazz. Chim. Ital. 83, 894–904.
Sami, D.G., Heiba, H.H., Abdellatif, A., 2019. Wound healing models: a systematic review of animal and non-animal models. Wound Med 24, 8–17. https://doi.org/10.1016/j.wndm.2018.12.001.
Sulasmi, I.S., 2012a. Jernang rattan (*Daemonorops draco*) management by Anak Dalam tribe in jebak village, batanghari, jambi province. J Biol Divers 13, 151–160. https://doi.org/10.13057/biodiv/d130309.
Sulasmi, I.S., 2012b. The population of jernang rattan (*Daemonorops draco*) in jebak village, batanghari district, jambi province, Indonesia. J Biol Divers 13, 205–213. https://doi.org/10.13057/biodiv/d130407.
Talapatra, B., Chaudhuri, P.K., Talapatra, S.K., 1982. (-)-Maglifloenone, a novel spirocyclohexadienone neolignan and other constituents form *Magnolia lilliflora*. Phytochemistry 21, 747–750. https://doi.org/10.1016/0031-9422(82)83180-4.
Todd, P.A., Faulds, D., 1991. Ofloxacin: a reappraisal of its antimicrobial activity, pharmacology and therapeutic use. Drugs 42 (5), 825–876.
Tsacheva, I., Rostan, J., Iossifova, T., Vogler, B., Odjakova, M., Navas, H., Kostova, I., Kojouharova, M., Kraus, W., 2004. Complement inhibiting properties of dragon' s blood from Croton draco. Z Naturforsch C J Biosci 59, 528–532. https://doi.org/10.1515/znc-2004-7-814.
Vermeulen, H., Westerbos, S.J., Ubbink, D.T., 2010. Benefit and harm of iodine in wound care: a systematic review. J. Hosp. Infect. 76, 191–199. https://doi.org/10.1016/j.jhin.2010.04.026.
Wahyuni, W.T., Purwanti, S., Batubara, I., 2018. Antibacterial and antibiofilm activity of *Daemonorops draco* resin. Biosaintifika J Biol Biol Educ 10, 138–144. https://doi.org/10.15294/biosaintifika.v10i1.13554.
Walcourt, A., Kurantsin-Mills, J., Kwagyan, J., Adenuga, B.B., Kalinowski, D.S., Lovejoy, D.B., Lane, J.R., Richardson, D.R., 2013. Anti-plasmodial activity of aroyl hydrazone and thiosemicarbazone iron chelators: effect on erythrocyte membrane integrity, parasite development and the intracellular labile iron pool. J. Inorg. Biochem. 129, 43–51. https://doi.org/10.1016/j.jinorgbio.2013.08.007.
Wang, G., Tang, C., Yan, G., Feng, B., 2016. Gene expression profiling of H9c2 cells subjected to H2O2-induced apoptosis with/without AF-hf001. Biol. Pharm. Bull. 39 (2), 207–214. https://doi.org/10.1248/bpb.b15-00601.
Wang, W., Nakashima, K.I., Hirai, T., Inoue, M., 2019. Neuroprotective effect of naturally occurring RXR agonists isolated from *Sophora tonkinensis* Gagnep. on amyloid-β-induced cytotoxicity in PC12 cells. J. Nat. Med. 73, 154–162. https://doi.org/10.1007/s11418-019-01305-8.
Wang, Y.Y., Yang, Y.X., Zhe, H., He, Z.X., Zhou, S.F., 2014. Bardoxolone methyl (CDDO-Me) as a therapeutic agent: an update on its pharmacokinetic and pharmacodynamic properties. Drug Des. Dev. Ther. 8, 2075–2088. https://doi.org/10.2147/DDDT.S68872.
Wardyn, J.D., Ponsford, A.H., Sanderson, C.M., 2015. Dissecting molecular cross-talk between Nrf2 and NF-κB response pathways. Biochem. Soc. Trans. 43, 621–626. https://doi.org/10.1042/BST20150014.
Wright, J.A., Richards, T., Srai, S.K., 2014. The role of iron in the skin and cutaneous wound healing. Front. Pharmacol. 5, 156. https://doi.org/10.3389/fphar.2014.00156.
Youn, G.S., Kwon, D.J., Ju, S.M., Rhim, H., Yong Soo Bae, Y.S., Choi, S.Y., Park, J., 2014. Celastrol ameliorates HIV-1 Tat-induced inflammatory responses via NF-kappaB and AP-1 inhibition and heme oxygenase-1 induction in astrocytes. Toxicol. Appl. Pharmacol. 280, 42–52. https://doi.org/10.1016/j.taap.2014.07.010.
Yunita, F., Mursyid, L., 2019. Acute toxicity test of jernang resin extract (*Daemonorops draco* willd.) on male white rats Sprague Dawley strain. Indones J Sci Technol 2 (2), 2615-367.
Zha, Z., Han, Q., Huo, S., 2020. The protective effects of bexarotene against advanced glycation end-product (AGE)-induced degradation of articular extracellular matrix (ECM). Artif Cells Nanomed Biotechnol 48 (1), 1–7. https://doi.org/10.1080/21691401.2019.1699802.
Zhao, R., Liang, H., Clarke, E., Jackson, C., Xue, M., 2016. Inflammation in chronic wounds. Int. J. Mol. Sci. 17, 2085. https://doi.org/10.3390/ijms17122085.
Ziltener, P., Reinheckel, T., Oxenius, A., 2016. Neutrophil and alveolar macrophage-mediated innate immune control of *Legionella pneumophila* lung infection via TNF and ROS. PLoS Pathog. 12, e1005591 https://doi.org/10.1371/journal.ppat.1005591.